Journal of Materials Chemistry A

ROYAL SOCIETY OF CHEMISTRY

COMMUNICATION

View Article Online
View Journal | View Issue

Cite this: J. Mater. Chem. A, 2021, 9, 15605

Received 14th May 2021
Accepted 17th June 2021

DOI: 10.1039/d1ta04084g

rsc.li/materials-a

Design of a unique anion framework in halospinels for outstanding performance of all solid-state Li-ion batteries: first-principles approach†

Hoje Chun, [a] Kyungju Nam,[bc] Sung Jun Hong, [a] Joonhee Kang *[d] and Byungchan Han *[ab]

A solid-state electrolyte (SSE) is a key component in the performance control of all-solid-state Li-ion batteries. The development of a promising material has, however, come to a standstill due to the undesirably low ionic conductivity and stability. Using first-principles calculations, we propose that halospinels, *i.e.*, $Li_2Sc_{2/3}X_4$ (X = Cl, Br, and I), should be encouraging materials to surmount the long-standing challenges. Density functional theory (DFT) calculations unveil their underlying mechanisms that the incorporated halogen anion and Sc form unique ionic pairs to create the atomic environment required for the dramatic facilitation of Li-ion diffusion to a superionic conductor level. In addition, collective ionic motions near the halogen species in the halospinel solid electrolyte promote the substantial enhancement of the electrochemical stability and interface compatibility with the electrodes. We demonstrate that a crucial factor is the rational selection of the halogen anion to achieve the maximal performance of the electrolyte. *Ab initio* molecular dynamics (AIMD) simulations consistently pinpoint that the halospinel with Cl anion, $Li_2Sc_{2/3}Cl_4$, is the best choice to maintain the high functionality of Li-ion conductivity, electrochemical stability, and interface compatibility with the $LiCoO_2$ electrode in Li-ion battery applications. Our study provides a fundamental ground on chemical design principles for a breakthrough in advancing solid-state electrolytes towards a wide commercialization of all-solid-state Li-ion batteries.

Introduction

All solid-state Li-ion batteries have attracted considerable interest as next-generation electric energy storage devices, due to the expected high chemical safety and energy density.[1–5] While they are promising, one of the key components, the solid-state electrolyte (SSE), has delayed their wide deployment into our society. The SSE shows inveterate challenges of undesired Li-ion conductivity and interfacial compatibility with electrodes in Li-ion battery operation. The minimal performance requirements to be competitive with conventional Li-ion battery systems are ionic conductivity higher than 1 mS cm^{-1}, electrochemical stability sustainable over 4 V (*vs.* Li/Li^+), and interface compatibility with electrodes.[6,7]

Over the last several decades, various types of SSEs were studied extensively, *i.e.*, sulfides[8,9] (*e.g.*, $Li_{10}GeP_2S_{12}$ and $Li_7P_3S_{11}$) and oxides[10,11] (*e.g.*, $Li_7La_3Zr_2O_{12}$ and $Li_{13}Al_{0.3}Ti_{1.7}P_3O_{12}$). Among these materials, sulfide electrolytes have drawn extra focus because of their super Li-ion conductivity (1–10 mS cm^{-1}), which is comparable to that of organic-based electrolytes.[12,13] In addition, the mechanical properties enabled more cost-effective synthesis and formation of appropriate interfaces with the electrodes compared to other counterparts.[14,15] Even so, the performance is still far below the commercialization target, predominantly due to the substantial property degradation when exposed to humid conditions.[16,17]

It is notable that chemical incorporation of halide anions into sulfide SSEs demonstrated enhanced stability because of the stronger oxidative property than chalcogenides.[18–20] Kato *et al.*[12] designed $Li_{9.54}Si_{1.74}P_{1.44}S_{11.7}Cl_{0.3}$ *via* Cl doping into $Li_{10}SiP_2S_{12}$, and observed higher Li-ion conductivity and phase stability than the pristine material. Arnold *et al.*[21] experimentally tested the electrochemical stability of argyrodite crystals, *i.e.*, Li_6PS_5X, with different halide dopants (X = Cl, Br, and I). Yet, the measurement of the stability attributed to the passivation layer and the homogeneity of the coating were rather insufficient to draw conclusive evidence, due to the small amounts of doping levels.

Recently, inspired by halide-doped sulfide ionic conductors, substantial investigations have been conducted on ionic conductors with entire halide anion frameworks[22–27] such as Li_3ErCl_6, Li_3YCl_6, and Li_3ZrCl_6. In the structures, Li-ions prefer

[a]Department of Chemical and Biomolecular Engineering, Yonsei University, Seoul 03722, Republic of Korea. E-mail: bchan@yonsei.ac.kr

[b]Department of Vehicle Convergence Engineering, Yonsei University, Seoul 03722, Republic of Korea

[c]Institute of Fundamental and Advanced Technology, R&D Division, Hyundai Motor Company, Uiwang 16082, Republic of Korea

[d]Platform Technology Laboratory, Korea Institute of Energy Research, Daejeon 34129, Republic of Korea. E-mail: j.kang@kier.re.kr

† Electronic supplementary information (ESI) available. See DOI: 10.1039/d1ta04084g

occupying octahedral sites to tetrahedral sites thermodynamically, the conductivity of which was tuned by controlling the phases or the Li compositions. It should be noted that a spinel-type superionic conductor,[28] *i.e.*, $Li_2Sc_{2/3}Cl_4$, was designed by a much easier process than other halide ionic conductors and demonstrated exceptionally high ionic conductivity, which could be attributed to the incorporated Cl by the formation of disordered cation (Li^+ and Sc^{3+}) structures to increase Li-ion occupancy. It was claimed that the high Li-ion concentrations in the halospinel should create three-dimensional diffusion paths through face-sharing octahedra and tetrahedra. Furthermore, multiple coupled incorporation of cationic or/and anionic species can be attempted to even more drive the performance, which may result in substantially unexpected performances as shown in other halide materials, *i.e.*, Li_3MX_6 (M = Sc, Y, In, and X = Cl, Br).[7]

Despite the meaningful studies, precise underlying principles and mechanisms of the unexpected performance are still immature for further improvement of SSE performance. They require a systematic and rigorous approach to identify any correlation between the halospinel electrolyte performance and halogen anions. Considering formidable degrees of freedom in the configuration and composition of the component species in the halospinel, pure experiments may not be practically suitable.[29–31]

In this paper, we effectively deal with the issues using first-principles density functional theory (DFT) calculations, integrated with *ab initio* molecular dynamics (AIMD) simulations. Using experimentally reported $Li_2Sc_{2/3}Cl_4$ as a parent halospinel SSE model, we studied how the incorporation of halogen anions (Cl, Br, and I) shifts the thermodynamic stability, ionic conductivity, and interfacial compatibility with electrodes in Li-ion batteries.

DFT calculations identified both energetically plausible configurational arrangements of Li and Sc atoms and Li-ion conductivity in the halospinels, *i.e.*, $Li_2Sc_{2/3}X_4$ (X = Cl, Br, and I), while AIMD simulations and statistical analyses uncover the microscopic mechanism of the diffusion of Li-ion. Our study characterized coupled collective motions of Li-ion diffusion in the halospinel, which plays a crucial role in the high ionic conductivity. In addition to the kinetic mechanism, the electrochemical potential regime for $Li_2Sc_{2/3}X_4$ stability and the interfacial reactions with an $LiCoO_2$ electrode were evaluated, and the improvement *via* halogen anion incorporation within the spinel was elucidated. We provide a clear atomistic ground that Cl is the best element for creating a unique anion framework in the halospinel, leading to superior Li-ion conductivity, electrochemical stability, and interface compatibility.

Computational methods

All of the DFT calculations were performed using the Vienna *ab initio* simulation package (VASP)[32,33] with the projector augmented wave (PAW)[34] pseudo-potential. The generalized gradient approximation (GGA) with Perdew–Burke–Ernzerhof (PBE)[35] was used to describe the exchange–correlation energy of the electrons. The plane-wave basis functions for the Kohn–Sham equation were expanded with the cutoff energy of 520 eV. The Brillouin zone in the reciprocal space was sampled by $4 \times 4 \times 1$ *k*-points with the Monkhorst–Pack scheme. The DFT calculations were stopped when the energy and force converged within 10^{-5} eV and 0.02 eV·Å^{-1}, respectively, with respect to the previous step. For the density of states (DOS) calculations, we utilized HSE06 hybrid functionals[36] to minimize the underestimation of GGA-PBE. The AIMD simulations were carried out using a Nosé–Hoover thermostat[37] in a statistical ensemble of a fixed particle number, volume, and temperature (NVT) conditions. The time-step of the simulations was set to 2 fs and 50 000 steps were performed at temperatures ranging from 600 to 1200 K with a Γ-point. The activation energy of the Li-ion diffusion along the assigned path was evaluated by the climbing-image nudged elastic band (CI-NEB) method.[38] Statistical analyses of the AIMD simulations were conducted using Pymatgen[30,39] in order to understand the Li-ion diffusion behavior. The chemical and electrochemical stabilities of SSE were evaluated using compositional and Li grand potential phase diagrams, respectively. We used the DFT energies of the corresponding compounds reported in the Materials Project open database,[40] and the compatibilities of the materials were estimated with the pseudo-binary model of the SSE and the electrode interface.[41–45]

Results and discussion

Model system and chemical stability

We constructed the model halospinel, $Li_2Sc_{2/3}Cl_4$, based on Li occupancy. The halospinel $Li_2Sc_{2/3}Cl_4$ has four symmetrically unequal Wyckoff sites for Li occupation, *i.e.*, 8a, 16c, 16d, and 48f (Fig. 1a and b).[46] The octahedra of $ScCl_6$ and $LiCl_6$ (Sc and Li in the 16d site) form an edge-sharing rhombus framework, while the octahedra of $LiCl_6$ (Li in 16c) and the tetrahedra of LiX_4 (Li in 8a and 48f) along Li-ion diffusion pathways share their faces. From the time-of-flight powder neutron diffraction analysis at 300 K,[28] the stoichiometry of $Li_2Sc_{2/3}Cl_4$ was identified as $Li_{17}Sc_5Cl_{32}$ in a conventional cell. In accordance with the report, we setup a model $Li_{17}Sc_5Cl_{32}$ for further calculations. For a simple notation, we express the stoichiometry of our halospinel systems as $Li_2Sc_{2/3}X_4$ (X = Cl, Br, and I). To efficiently construct the computational models of the halospinels, we hypothesized that appropriate configurations of Li and Sc ions are significant because Sc ions are immobile during the diffusion process, while the arrangements of other Li ions at different Wyckoff sites are marginal since they diffuse through the channels. We identified a total of 35 model systems satisfying the configurations of Li and Sc at 16d sites with the occupancies of Li: 0.6875 and Sc: 0.3125 and used them for the $Li_2Sc_{2/3}X_4$ structural analysis (Fig. S1†).[47]

Regardless of the types of incorporated halide anions, our DFT calculations indicate that the distributions of stability for the 35 models are similar, and the positions of Li and Sc atoms are also the same for the most stable and unstable structures. Thermodynamically, the most stable structure (model 13) shows that Li and Sc atoms are well distributed in the rhombus coordination framework (Fig. 1c), while in the most unstable

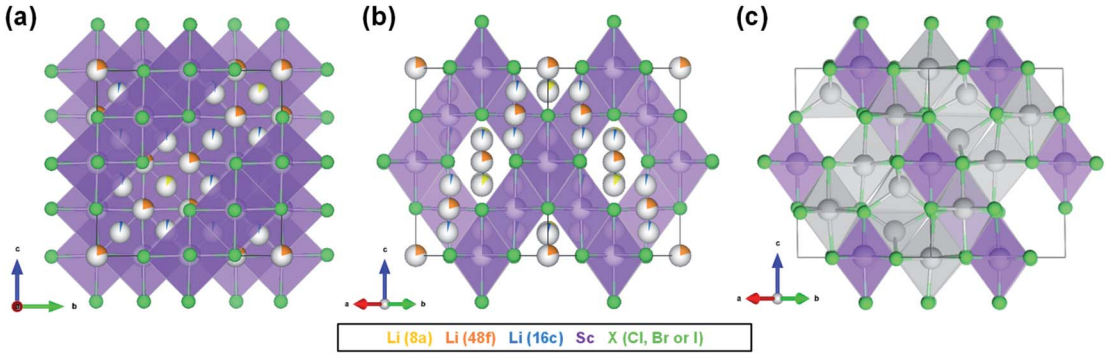

Fig. 1 Model systems of $Li_2Sc_{2/3}X_4$: (a) and (b) $Li_2Sc_{2/3}X_4$ with different Wyckoff sites 8a, 48f, and 16c for Li occupation and 16d for both Li and Sc accommodation. (c) The most stable structure thermodynamically.

structure (model 26) Li atoms are present in close proximity among each other (Fig. S2†). It shows that the rigid connectivity of the face-sharing octahedra and tetrahedra is better for the structural integrity of the halospinels.

As depicted in Fig. S3,† we identified the lattice symmetry ($Fd\bar{3}m$) of $Li_2Sc_{2/3}Cl_4$, $Li_2Sc_{2/3}Br_4$, and $Li_2Sc_{2/3}I_4$ using DFT calculations, which well agrees with the experimental observations.[28] The highest and the second highest intensity peaks appearing at 33.9° and 29.2° correspond to the (122) and (004) planes, respectively. $Li_2Sc_{2/3}Br_4$ and $Li_2Sc_{2/3}I_4$ also show similar structural features to $Li_2Sc_{2/3}Cl_4$. The slight downshifts of the peak positions are due to elongated bond lengths of Sc–X as the halide (X) ionic radius increases.

The chemical stability of $Li_2Sc_{2/3}X_4$ was affirmed further by formation energy calculations, as described in eqn (1) and (2).

$$2Li + 2/3Sc + 2X_2 = Li_2Sc_{2/3}X_4 \quad (1)$$

$$\Delta E_{formation} = E_{Li_2Sc_{2/3}X_4} - 2E_{Li} - 2/3E_{Sc} - 2E_{X_2} \quad (2)$$

$E_{Li_2Sc_{2/3}X_4}$, E_{Li}, E_{Sc}, and E_{X_2} are the mean DFT energies for each ground state structure of $Li_2Sc_{2/3}X_4$, Li, Sc, and halogen gaseous molecules, respectively. In a formula unit, the formation energies were calculated as −12.77, −9.85, and −7.00 eV for $Li_2Sc_{2/3}Cl_4$, $Li_2Sc_{2/3}Br_4$, and $Li_2Sc_{2/3}I_4$, respectively. The results indicate that $Li_2Sc_{2/3}Cl_4$ is by far more stable. The stability was evaluated further using the Li–Sc–X_2 phase diagrams as shown in Fig. S4.† Along with $Li_2Sc_{2/3}Cl_4$, both $Li_2Sc_{2/3}Br_4$ and $Li_2Sc_{2/3}I_4$ are predicted to be thermodynamically stable with respect to their own reference states, implying that our model systems of $Li_2Sc_{2/3}X_4$ can be experimentally synthesized.

Li-ionic conductivity in halospinels

The diffusion coefficient of $Li_2Sc_{2/3}X_4$ at 300 K was obtained by the linear extrapolation of higher temperature (600–1200 K) values calculated by AIMD simulations (Fig. 2a–c). Li-ionic conductivity and the activation energy of Li-ion migration in $Li_2Sc_{2/3}X_4$ were calculated using the Nernst–Einstein equation and Arrhenius plot by the least-squares method. The error bounds of activation barriers were obtained from the residuals of the least-squares method. Ionic conductivities of $Li_2Sc_{2/3}Cl_4$, $Li_2Sc_{2/3}Br_4$, and $Li_2Sc_{2/3}I_4$ were 2.07, 0.20 and 2.78 mS cm^{-1}, respectively. Notably, $Li_2Sc_{2/3}Cl_4$ and $Li_2Sc_{2/3}I_4$ show outstanding Li-ion conductivities comparable to a superionic conductor (10^{-3}–10^{-2} S cm^{-1}), while $Li_2Sc_{2/3}Br_4$ is a poor conductor of Li ions. The results are in good agreement with the activation energies, in which $Li_2Sc_{2/3}Br_4$ has the highest value (0.366 eV).

Fig. 2d–f show the probability density map of Li-ion diffusion in $Li_2Sc_{2/3}Cl_4$, $Li_2Sc_{2/3}Br_4$, and $Li_2Sc_{2/3}I_4$. All of them exhibit the three-dimensional network for Li diffusion, as represented by the yellow isosurface. It is noteworthy that the probability density plot for isosurfaces of $Li_2Sc_{2/3}Cl_4$ shows the tightest connectivity among the three halospinels, which favorably promotes the collective Li-ion motion. As a quick guess, the incorporation of a more polarizable halogen anion should improve the ionic conductivity due to the well-known lattice softening effect.[7,46] Nonetheless, Cl is more preferred to Br and I on the aspect of stability.

Interestingly, Cl, in fact, does not degrade the Li-ion conductivity of the $Li_2Sc_{2/3}X_4$ halospinel, but rather is a better choice than Br, which is thought to be more polarizable than Cl. To unveil the underlying principle of the unexpectedly good ionic conductivity of $Li_2Sc_{2/3}Cl_4$, which is not well explained by conventional chemical theories, we investigated Li-ion diffusion in $Li_2Sc_{2/3}X_4$ for two different cases: (1) a single ion hopping and (2) a collective motion of Li-ions along the diffusion channels.

For the first, we calculated the anion polarizability and charges for the Li-ion diffusion process. In Table 1, the volumetric polarizability (χ)[48] was calculated using eqn (3).

$$\chi = \left(\frac{V}{4\pi}\right)(\varepsilon - 1) \quad (3)$$

here, V is the volume of an $Li_2Sc_{2/3}X_4$ per Sc atom and ε is a high frequency dielectric constant. Overall, the volumetric polarizability was obtained by averaging the tensor components of χ_{xx}, χ_{yy}, and χ_{zz}. It turned out that $Li_2Sc_{2/3}I_4$ had the largest value (69.54 $Å^3$), and it was followed by $Li_2Sc_{2/3}Br_4$ (41.20 $Å^3$) and $Li_2Sc_{2/3}Cl_4$ (28.18 $Å^3$). These different polarizabilities could cause uneven equilibrium volumes and therefore uneven pore sizes of the halospinels. Using the Zeo++ program,[49] we identified that the average pore sizes were in the order of $Li_2Sc_{2/3}I_4$ (2.45 Å) > $Li_2Sc_{2/3}Br_4$ (2.25 Å) > $Li_2Sc_{2/3}Cl_4$ (2.09 Å).

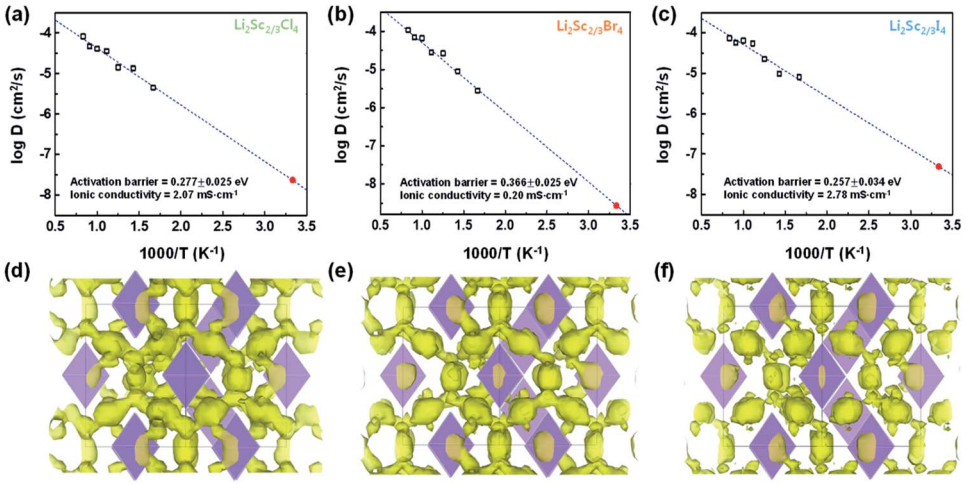

Fig. 2 Calculated Li-ion diffusivity at 300 K (red circles) of (a) $Li_2Sc_{2/3}Cl_4$, (b) $Li_2Sc_{2/3}Br_4$, and (c) $Li_2Sc_{2/3}I_4$. Probability density plot of a diffusing Li-ion at 800 K for (d) $Li_2Sc_{2/3}Cl_4$, (e) $Li_2Sc_{2/3}Br_4$, and (f) $Li_2Sc_{2/3}I_4$.

Table 1 Polarizability volume, pore size for Li diffusion, and the ratio of charge and tetrahedron bonding with varying incorporated halogen elements

	Average polarizability volume (Å^3)	Average pore size (Å)	$\frac{\lvert q_X\rvert}{d_{tet}}$ (e Å^{-1})
$Li_2Sc_{2/3}Cl_4$	28.18	2.09	0.34
$Li_2Sc_{2/3}Br_4$	41.20	2.25	0.31
$Li_2Sc_{2/3}I_4$	69.54	2.45	0.28

Furthermore, we estimated the activation energy (E_a) for Li-ion migration by the relative anionic charge to Li–X bond lengths in the tetrahedron, $\frac{\lvert q_X\rvert}{d_{tet}}$. As dictated by eqn (4),[50] larger the $\frac{\lvert q_X\rvert}{d_{tet}}$, higher the activation energy.

$$E_a \propto E_{oct} - E_{tet} \approx C + \frac{Ae^2}{4\pi\varepsilon}\left(\frac{\lvert q_X\rvert}{d_{tet}}\right) \quad (4)$$

where C and A are positive constants. Our calculations indicate that $\frac{\lvert q_X\rvert}{d_{tet}}$ are in the order of $Li_2Sc_{2/3}Cl_4 > Li_2Sc_{2/3}Br_4 > Li_2Sc_{2/3}I_4$, and therefore, among the three halospinels, $Li_2Sc_{2/3}Cl_4$ has the largest activation energy for Li-ion diffusion.

Both the pore size and the activation energy of $Li_2Sc_{2/3}X_4$ suggest that the incorporation of Cl would not be a good choice for high Li-ion conductivity. This is strikingly inconsistent with what AIMD simulations represent. The critical issue is attributed to the insufficient analysis by the single Li ion diffusion neglecting the influence of the collective ionic motions.

Previous studies[51,52] reported that the collective movements of ions can substantially modify the kinetic motion behavior of a single particle. Sun *et al.*[26] examined the Li-ion hopping mechanism in Li_xScCl_{3+x} as a function of Li concentration, but no explicit evidence for the concerted lattice movement was identified. Accordingly, we investigated the collective motion of Li ions through the channels. For our halospinels, we calculated the van Hove correlation function to detect any collective Li-ion motion. Considering the self-part of the van Hove correlation function (G_s) in $Li_2Sc_{2/3}X_4$ (Fig. 3a–c), the Li-ions in $Li_2S_{2/3}Cl_4$ should have the lowest probability for returning to their original positions and shortest stay at the position among the halospinels. The distinct-part (G_d) shows the correlation time scale of the Li-ion motions. As shown in Fig. 3d–f, the correlation time of $Li_2Sc_{2/3}Cl_4$ (G_d around $r = 0$ Å) indicates a high correlation of Li-ion motion. However, the correlation time increases for $Li_2Sc_{2/3}Br_4$ and $Li_2Sc_{2/3}I_4$, implying a stronger collective Li-ion migration in $Li_2Sc_{2/3}Cl_4$. Furthermore, the Haven ratios of $Li_2Sc_{2/3}Cl_4$, $Li_2Sc_{2/3}Br_4$, and $Li_2Sc_{2/3}I_4$ were computed as 2.40, 0.51, and 0.97, respectively, which also substantiates the high correlation of Li-ion motions in $Li_2Sc_{2/3}Cl_4$ (Table S1†). These facts clearly suggest that the collective ionic motions in the halospinels strongly influence the ionic conductivity, which substantially varies depending on the incorporated halogen anions.

Using the CI-NEB method, we quantitatively evaluated the activation energy of the concerted Li-ion diffusion (Fig. 3g). In the process, we initially placed two Li-ions at the same Wyckoff site (8a) along the face-sharing octahedra and tetrahedra pathway (Fig. 3h). Li–Li interaction is marginal until the first Li (Li1) hops into the 48f site, where the second Li (Li2) starts to experience a repulsive force. Then, Li2 hops to the next 48f site, and this is followed by Li1 hopping into 8a, where Li2 was initially located. These characteristics are substantiated by the appearance of two peaks along the diffusion path, as shown in Fig. 3g. Our results indicated that Li-ions in $Li_2Sc_{2/3}Cl_4$, $Li_2Sc_{2/3}Br_4$, and $Li_2Sc_{2/3}I_4$ have different activation barriers of 0.9, 1.1, and 1.0 eV, respectively. The overestimation of the activation barriers from the CI-NEB method is mainly attributed to the restriction of the Li-ion diffusing channel as we considered that only two Li-ions move along the channel. The collective motion behavior of the Li-ion is consistent with the calculated ionic conductivity of $Li_2Sc_{2/3}X_4$ at room temperature. Thus, we

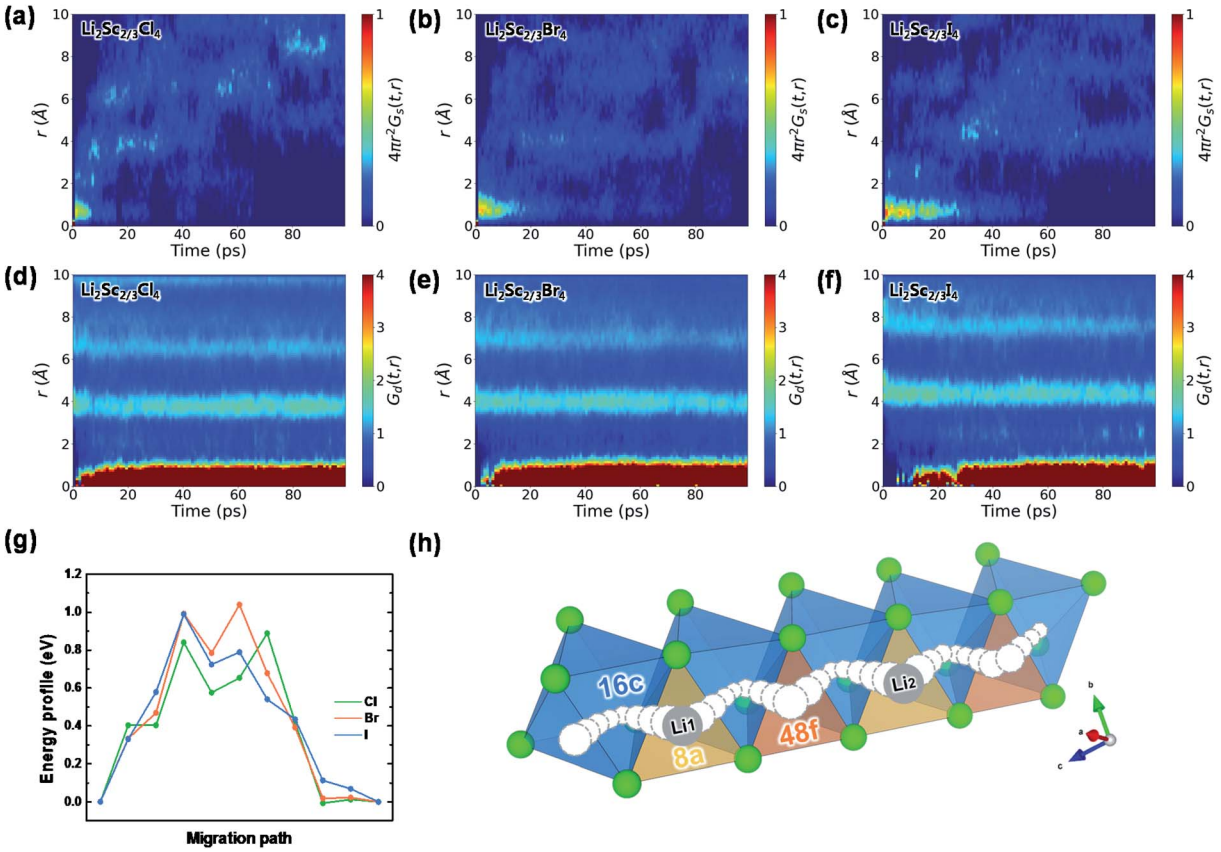

Fig. 3 (a–c) The self-part (G_s) and (d–f) the distinct-part (G_d) of the van Hove correlation functions for Li-ion motion at 800 K in $Li_2Sc_{2/3}Cl_4$, $Li_2Sc_{2/3}Br_4$, and $Li_2Sc_{2/3}I_4$. (g) The migration energy barriers of concerted Li-ion motion along (h) the face-sharing octahedra and tetrahedra pathway.

propose that the collective motion of Li-ions through the diffusion channels is critical to accurately describe the outstanding ionic conductivity. The underlying mechanism of the collective motion was further investigated from the effective coordination numbers (ECoNs) for the polyhedron of Li in 8a and 16d sites. As previously proposed,[53] a smaller ECoN implies a larger structural distortion of the Li-polyhedron, inducing fast ionic diffusion. Our calculations indicate that the average ECoN of Li in 8a for $Li_2Sc_{2/3}Cl_4$ has the largest distortion, although the difference is marginal ($Li_2Sc_{2/3}Cl_4$: 3.79, $Li_2Sc_{2/3}Br_4$: 3.79, and $Li_2Sc_{2/3}I_4$: 3.83). Interestingly, the gap of distortions among the three halospinels for the Li-polyhedron in 16d was noticeably increased ($Li_2Sc_{2/3}Cl_4$: 5.26, $Li_2Sc_{2/3}Br_4$: 5.42, and $Li_2Sc_{2/3}I_4$: 5.45). Accordingly, the reason for the highly collective Li-ion motion in $Li_2Sc_{2/3}Cl_4$ is ascribed to the large structural distortion of the Li-polyhedron in the 16d site. The effect can be further reinforced by increasing the Li amount in the face-sharing polyhedra.

Our results clearly indicate that an incautious conjecture based on individually uncorrelated ionic motion may fail in the accurate prediction of dynamic material properties. In halospinels the collective Li-ionic motions are crucial for precise description of ionic conductivity, which can be tuned using the incorporated halogen anion. Our results propose that multiple anion doping into halospinels can be imagined for even more conductive SSE materials. In searching for optimum species and appropriate concentrations of the dopants our study should be useful as a good starting guide.

Electrochemical stability of halospinels

For an SSE to be a promising component of a solid-state Li-ion battery it should be stable at the operating electrochemical potentials and demonstrate good interface compatibility with electrodes.[43] First, we calculated the DOS of all $Li_2Sc_{2/3}X_4$ models, as depicted in Fig. S5.† The band gaps of $Li_2Sc_{2/3}Cl_4$, $Li_2Sc_{2/3}Br_4$, and $Li_2Sc_{2/3}I_4$ are 5.79, 4.80, and 3.83 eV, respectively, and all conduction band minima (CBM) originate from the ScX_6 (X = Cl, Br, or I) octahedra.

The electrochemical stability of the halospinels was evaluated by calculating phase equilibria as a function of applied potential (referenced to the Li/Li^+ electrode). As shown in Fig. 4a–c, all three halospinels show wide electrochemical potential windows with anodic upper limits of 4.25, 3.14, and 2.47 V and cathodic lower limits of 0.91, 0.93, and 1.11 V, respectively. The halospinels suffer from electrochemical oxidation by the incorporated halogen anions at above the anodic potential limit, leading to the formation of ScX_3 and X_2. In contrast, electrochemical reduction reactions by Sc ions proceed at potentials below the cathodic limit, resulting in LiX

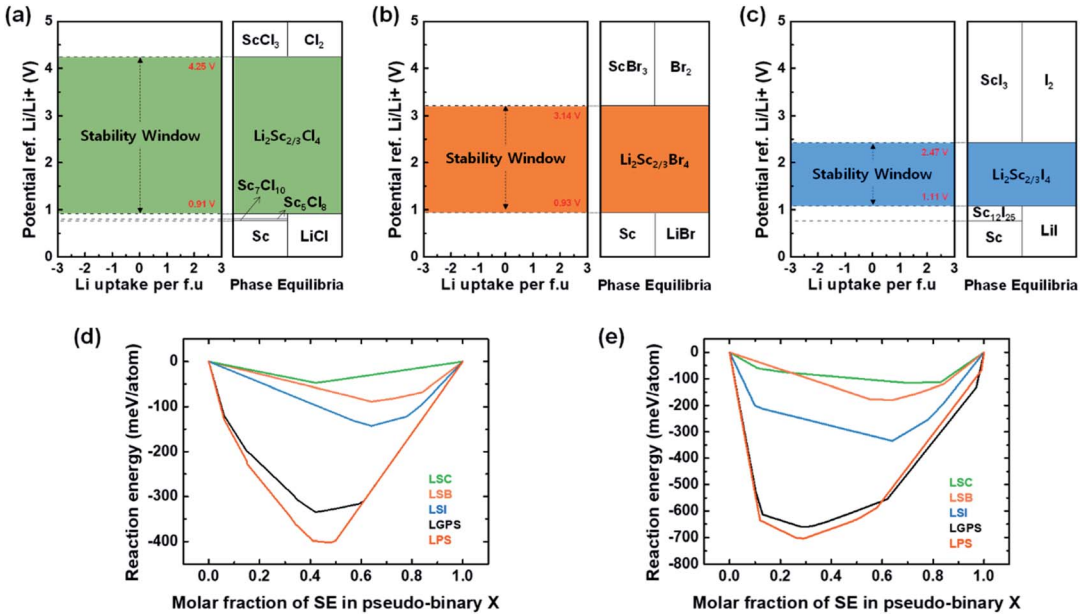

Fig. 4 Thermodynamic voltage profile and phase equilibria: (a) for $Li_2Sc_{2/3}Cl_4$, (b) for $Li_2Sc_{2/3}Br_4$, and (c) for $Li_2Sc_{2/3}I_4$, respectively. Calculated mutual reaction energy of the SSE–$LiCoO_2$ interface in (d) and in (e) the mutual reaction energy at an applied potential of 3 V.

and Sc-X compounds. The electrochemical stability of $Li_2Sc_{2/3}X_4$ estimated with the potential window is better than that of many conventionally known sulfide SSEs, such as $Li_{10}GeP_2S_{12}$ (1.72–2.29 V), and Li_3PS_4 (1.71–2.31 V). Especially, the stability of $Li_2Sc_{2/3}Cl_4$ is remarkable compared to that of Br- and I-spinels.

To investigate the interfacial compatibility of the halospinels with electrodes, we used $LiCoO_2$ as a cathode model. The chemical reaction energy at the interface of $Li_2Sc_{2/3}X_4$ and $LiCoO_2$ was calculated *via* a pseudo-binary model.[41] As shown in Fig. 4d and Table S2–S4,† the interfacial reaction energies of $Li_{10}GeP_2S_{12}$ and Li_3PS_4 (*i.e.*, −442 and −335 meV per atom, respectively) imply that they are thermodynamically not stable, which agrees with previous reports. In contrast, all three halospinels of $Li_2Sc_{2/3}X_4$ are significantly more stable than the two electrolytes (interfacial reaction energies of −49, −89, and −143 meV per atom, respectively). This can be explained by the fact that the Li–Sc–Cl chemical bond has high coulombic efficiency, and therefore $Li_2Sc_{2/3}Cl_4$ is more electrochemically stable at the interface with $LiCoO_2$ than the other two halospinels. In addition, $Li_2Sc_{2/3}Cl_4$ is chemically inert to interface reactions at the potential of 3 V (Fig. 4e and Table S5–S7†).

To summarize, the incorporation of Cl was the best choice among the three halogen species for designing high performance halospinel $Li_2Sc_2X_4$ in solid-state Li-ion battery applications. This is mostly because it forms an ion pair with Sc which is chemically more desirable because it enhances both the Li-ion conductivity and the chemical stability. The incorporated Cl in the $Li_2Sc_{2/3}X_4$ halospinel drives concerted ionic Li motions leading to substantial facilitation of Li-ion diffusion. It violates the conventional hypothesis based on polarizability effects which would go for Br and I instead. Based on the results, we propose a design principle that the activation of the concerted motions of Li-ion is crucial for highly ionic conductive SSEs, which can be easily tuned by single or multiple incorporation of anions in spinels.

Conclusions

Using first-principles DFT calculations we have unveiled the fundamental design principles and mechanisms for high performance halospinels, *i.e.*, $Li_2Sc_{2/3}X_4$ (X = Cl, Br, and I), for ionic conductors. Depending on the substitutionally incorporated halogen anion, the performance was strikingly shifted. Using XRD patterns, the chemical phase diagram, and the formation energy of each halospinel, we consistently affirmed the findings. The Li-ion conductivities of $Li_2Sc_{2/3}Cl_4$ and $Li_2Sc_{2/3}I_4$ were comparable to those of conventionally known superionic conductors, >2 mS m^{-1}. Contrastingly different mechanisms were, however, identified for the two spinels: $Li_2Sc_{2/3}Cl_4$ exhibited much better activation of highly correlated and collective diffusion of Li-ions, while the Li-ion conductivity in $Li_2Sc_{2/3}I_4$ was predominantly contributed by the polarizable anion framework. All three halospinels showed much better interfacial compatibility with the $LiCoO_2$ cathode than the conventionally known sulfides $Li_{10}GeP_2S_{12}$ and Li_3PS_4 SSEs. $Li_2Sc_{2/3}Cl_4$, however, demonstrated superior electrochemical stability. Our study essentially demonstrates that the incorporation of properly selected halogen species into spinel SSEs is essential for the performance manifestation, and Cl is an outstanding choice for the purpose due to its unique Sc–Cl cation–anionic pair in the halospinel $Li_2Sc_{2/3}Cl_4$.

Author contributions

H. C., K. N., J. K., and B. H. conceived the idea. H. C. K. N., and J. K. performed the DFT calculations. H. C., K. N., and S. H.

analyzed the data. H. C., J. K., and B. H. wrote the manuscript, and all authors discussed the results.

Conflicts of interest

There are no conflicts to declare.

Acknowledgements

This work was supported by the Global Frontier Program through the Global Frontier Hybrid Interface Materials (GFHIM) of the NRF funded by the Ministry of Science and ICT (project no. 2013M3A6B1078882) and by the Research and Development Program of KIER (C1-2447) in the Republic of Korea.

Notes and references

1 J. Janek and W. G. Zeier, *Nat. Energy*, 2016, **1**, 1–4.
2 Z. Gao, H. Sun, L. Fu, F. Ye, Y. Zhang, W. Luo and Y. Huang, *Adv. Mater.*, 2018, **30**, 1705702.
3 Y.-S. Hu, *Nat. Energy*, 2016, **1**, 1–2.
4 Z. Zhang, Y. Shao, B. Lotsch, Y.-S. Hu, H. Li, J. Janek, L. F. Nazar, C.-W. Nan, J. Maier and M. Armand, *Energy Environ. Sci.*, 2018, **11**, 1945–1976.
5 Y. Meesala, A. Jena, H. Chang and R.-S. Liu, *ACS Energy Lett.*, 2017, **2**, 2734–2751.
6 A. Manthiram, X. Yu and S. Wang, *Nat. Rev. Mater.*, 2017, **2**, 1–16.
7 T. Zhang, W. He, W. Zhang, T. Wang, P. Li, Z. Sun and X. Yu, *Chem. Sci.*, 2020, **11**, 8686–8707.
8 N. Kamaya, K. Homma, Y. Yamakawa, M. Hirayama, R. Kanno, M. Yonemura, T. Kamiyama, Y. Kato, S. Hama and K. Kawamoto, *Nat. Mater.*, 2011, **10**, 682–686.
9 I.-H. Chu, H. Nguyen, S. Hy, Y.-C. Lin, Z. Wang, Z. Xu, Z. Deng, Y. S. Meng and S. P. Ong, *ACS Appl. Mater. Interfaces*, 2016, **8**, 7843–7853.
10 R. Murugan, V. Thangadurai and W. Weppner, *Angew. Chem., Int. Ed.*, 2007, **46**, 7778–7781.
11 H. Aono, E. Sugimoto, Y. Sadaoka, N. Imanaka and G.-y. Adachi, *Solid State Ionics*, 1990, **40**, 38–42.
12 Y. Kato, S. Hori, T. Saito, K. Suzuki, M. Hirayama, A. Mitsui, M. Yonemura, H. Iba and R. Kanno, *Nat. Energy*, 2016, **1**, 1–7.
13 S. Muy, J. C. Bachman, L. Giordano, H.-H. Chang, D. L. Abernathy, D. Bansal, O. Delaire, S. Hori, R. Kanno and F. Maglia, *Energy Environ. Sci.*, 2018, **11**, 850–859.
14 A. Sakuda, A. Hayashi and M. Tatsumisago, *Sci. Rep.*, 2013, **3**, 1–5.
15 Q. Liu, Z. Geng, C. Han, Y. Fu, S. Li, Y.-b. He, F. Kang and B. Li, *J. Power Sources*, 2018, **389**, 120–134.
16 J. M. Doux, H. Nguyen, D. H. Tan, A. Banerjee, X. Wang, E. A. Wu, C. Jo, H. Yang and Y. S. Meng, *Adv. Energy Mater.*, 2020, **10**, 1903253.
17 K. J. Kim, M. Balaish, M. Wadaguchi, L. Kong and J. L. Rupp, *Adv. Energy Mater.*, 2021, **11**, 2002689.
18 D. H. Tan, E. A. Wu, H. Nguyen, Z. Chen, M. A. Marple, J.-M. Doux, X. Wang, H. Yang, A. Banerjee and Y. S. Meng, *ACS Energy Lett.*, 2019, **4**, 2418–2427.
19 J. Kang and B. Han, *J. Phys. Chem. Lett.*, 2016, **7**, 2671–2675.
20 K. Nam, H. Chun, J. Hwang and B. Han, *ACS Sustainable Chem. Eng.*, 2020, **8**, 3321–3327.
21 W. Arnold, D. A. Buchberger, Y. Li, M. Sunkara, T. Druffel and H. Wang, *J. Power Sources*, 2020, **464**, 228158.
22 K.-H. Park, K. Kaup, A. Assoud, Q. Zhang, X. Wu and L. F. Nazar, *ACS Energy Lett.*, 2020, **5**, 533–539.
23 X. Li, J. Liang, J. Luo, M. N. Banis, C. Wang, W. Li, S. Deng, C. Yu, F. Zhao and Y. Hu, *Energy Environ. Sci.*, 2019, **12**, 2665–2671.
24 T. Asano, A. Sakai, S. Ouchi, M. Sakaida, A. Miyazaki and S. Hasegawa, *Adv. Mater.*, 2018, **30**, 1803075.
25 R. Schlem, S. Muy, N. Prinz, A. Banik, Y. Shao-Horn, M. Zobel and W. G. Zeier, *Adv. Energy Mater.*, 2020, **10**, 1903719.
26 J. Liang, X. Li, S. Wang, K. R. Adair, W. Li, Y. Zhao, C. Wang, Y. Hu, L. Zhang, S. Zhao, S. Lu, H. Huang, R. Li, Y. Mo and X. Sun, *J. Am. Chem. Soc.*, 2020, **142**, 7012–7022.
27 H. Kwak, D. Han, J. Lyoo, J. Park, S. H. Jung, Y. Han, G. Kwon, H. Kim, S. T. Hong and K. W. Nam, *Adv. Energy Mater.*, 2021, 2003190.
28 L. Zhou, C. Y. Kwok, A. Shyamsunder, Q. Zhang, X. Wu and L. F. Nazar, *Energy Environ. Sci.*, 2020, **13**, 2056–2063.
29 A. M. Nolan, Y. Zhu, X. He, Q. Bai and Y. Mo, *Joule*, 2018, **2**, 2016–2046.
30 Y. Mo, S. P. Ong and G. Ceder, *Chem. Mater.*, 2012, **24**, 15–17.
31 X. He, Y. Zhu, A. Epstein and Y. Mo, *npj Comput. Mater.*, 2018, **4**, 1–9.
32 G. Kresse and J. Furthmüller, *Phys. Rev. B: Condens. Matter Mater. Phys.*, 1996, **54**, 11169.
33 G. Kresse and J. Hafner, *Phys. Rev. B: Condens. Matter Mater. Phys.*, 1993, **47**, 558.
34 P. E. Blöchl, *Phys. Rev. B: Condens. Matter Mater. Phys.*, 1994, **50**, 17953.
35 J. P. Perdew, K. Burke and M. Ernzerhof, *Phys. Rev. Lett.*, 1996, **77**, 3865.
36 J. Heyd, G. E. Scuseria and M. Ernzerhof, *J. Chem. Phys.*, 2003, **118**, 8207–8215.
37 W. G. Hoover, *Phys. Rev. A: At., Mol., Opt. Phys.*, 1985, **31**, 1695.
38 G. Henkelman and H. Jónsson, *J. Chem. Phys.*, 2000, **113**, 9978–9985.
39 S. P. Ong, Y. Mo, W. D. Richards, L. Miara, H. S. Lee and G. Ceder, *Energy Environ. Sci.*, 2013, **6**, 148–156.
40 A. Jain, S. P. Ong, G. Hautier, W. Chen, W. D. Richards, S. Dacek, S. Cholia, D. Gunter, D. Skinner and G. Ceder, *APL Mater.*, 2013, **1**, 011002.
41 L. J. Miara, W. D. Richards, Y. E. Wang and G. Ceder, *Chem. Mater.*, 2015, **27**, 4040–4047.
42 Y. Zhu, X. He and Y. Mo, *ACS Appl. Mater. Interfaces*, 2015, **7**, 23685–23693.
43 Y. Zhu, X. He and Y. Mo, *J. Mater. Chem. A*, 2016, **4**, 3253–3266.

44 F. Han, Y. Zhu, X. He, Y. Mo and C. Wang, *Adv. Energy Mater.*, 2016, **6**, 1501590.
45 S. P. Ong, L. Wang, B. Kang and G. Ceder, *Chem. Mater.*, 2008, **20**, 1798–1807.
46 J. Liang, X. Li, K. R. Adair and X. Sun, *Acc. Chem. Res.*, 2021, **54**, 1023–1033.
47 K. Okhotnikov, T. Charpentier and S. Cadars, *J. Cheminf.*, 2016, **8**, 1–15.
48 S. J. Hong, H. Chun, K.-A. Min and B. Han, *J. Mater. Chem. C*, 2020, **8**, 9540–9548.
49 M. Pinheiro, R. L. Martin, C. H. Rycroft, A. Jones, E. Iglesia and M. Haranczyk, *J. Mol. Graphics Modell.*, 2013, **44**, 208–219.
50 Z. Xu, X. Chen, K. Liu, R. Chen, X. Zeng and H. Zhu, *Chem. Mater.*, 2019, **31**, 7425–7433.
51 X. He, Y. Zhu and Y. Mo, *Nat. Commun.*, 2017, **8**, 1–7.
52 J. Kang, H. Chung, C. Doh, B. Kang and B. Han, *J. Power Sources*, 2015, **293**, 11–16.
53 W. Zhang, D.-H. Seo, T. Chen, L. Wu, M. Topsakal, Y. Zhu, D. Lu, G. Ceder and F. Wang, *Science*, 2020, **367**, 1030–1034.